Oil & Natural Gas Technology

DOE Award No.: DE-FC26-06NT43067

Quarterly Progress Report (January – March 2010)

Mechanisms Leading to Co-Existence of Gas and Hydrate in Ocean Sediments

Submitted by:
Massachusetts Institute of Technology
77 Massachusetts Avenue, Room 48-319
Cambridge, MA 02139
and
The University of Texas at Austin
1 University Station C0300
Austin, TX 78712-0228

Prepared for:
United States Department of Energy
National Energy Technology Laboratory

March 31, 2010

Office of Fossil Energy

MECHANISMS LEADING TO CO-EXISTENCE OF GAS AND HYDRATE IN OCEAN SEDIMENTS

CONTRACT NO. DE-FC26-06NT43067

Deliverable 7.2:
Report on Task 7.0 "Coupled gas/water/sediment dynamics with hydrate formation," Subtask 7.2 "Coupled dynamics with fragile hydrate films"

March 31, 2010

Prepared by

Ruben Juanes
Department of Civil and Environmental Engineering
Massachusetts Institute of Technology
77 Massachusetts Avenue, Room 48-319
Cambridge, MA 02139
Phone: (617)253-7191
Email: juanes@mit.edu
and
Steven L. Bryant
Department of Petroleum and Geosystems Engineering
The University of Texas at Austin
1 University Station C0300
Austin, TX 78712-0228
Phone: (512) 471 3250
Email: steven_bryant@mail.utexas.edu

Prepared for
U.S. Department of Energy - NETL
3610 Collins Ferry Road
P.O. Box 880
Morgantown, WV 26508

Acknowledgment: "This material is based upon work supported by the Department of Energy under Award Number DE-FC26-06NT43067."

7.2 Coupled dynamics with fragile hydrate films: grain-scale model

We study the migration of methane gas within marine sediments under hydrate-forming conditions. A grain-scale model for drainage of water by gas invasion is used to estimate the location of the gas-water interface. This knowledge allows evaluation of the extent of hydrate formation within the pore space, over relatively short time period. Our model includes account of inelastic mechanical deformations of the sediment by grain rearrangements and intergranular deformations. As a consequence, the model describes two drainage mechanisms: (a) capillary invasion and (b) fracturing. Here, fracturing refers to opening of preferential flow paths by intergranular displacements as gas pressures overcome the intergranular stresses within the sediment matrix.

We consider episodic recharge of gas into the sediment, typical in many geological systems [Haeckel *et al*., 2004; Hester and Brewer, 2009], and describe the subsequent meniscus adjustments and hydrate formation that occurs prior to an additional gas recharge event. Thus, our results relate to the short-term distribution of the methane phases, over time scales which are much shorter than the characteristic time between recharge events. Since the timescale associated with hydrate formation (including nucleation) is much larger than that of gas-water interface adjustments following a pressure jump, we model formation of a thin hydrate film along a static interface, after it has attained its equilibrium position for the current capillary pressure.

Following nucleation of hydrate crystals, which occurs preferentially at the gas-water meniscus, a thin hydrate layer quickly spreads across the meniscus, restricting further reaction due to mass transfer limitations [Ribeiro and Lage, 2008; Sloan and Koh, 2008; Sum *et al*., 2009; Taylor *et al*., 2007]. With time, the hydrate film becomes thicker and denser, and the reaction slows down considerably [Taylor *et al*., 2007]. Several mechanisms have been proposed for the renewal of the gas-water interface–by mass transfer of the reactants across the hydrate film–including diffusion of gas [Taylor *et al*., 2007] and permeation of water [Davies *et al*., 2010].

Here, we propose an alternative mechanism: mechanical instability of the hydrate shell. Our hypothesis is based on observations of collapse of the hydrate shell over short time scales of seconds after hydrate completely covered gas bubbles [Gumerov and Chahine, 1998; Sun *et al*., 2007]. We assume a similar failure to occur in the weakest parts of a hydrate film that grows around within sediments. Considering a finite body of gas which is not recharged by an external source, the instability arises because of the gas pressure drop associated with the consumption of methane as it is converted to hydrate (Figure 1). In our model, the hydrate-shelled gas body implodes if the difference between the gas and water pressure (assumed to remain hydrostatic) drops below a critical value. Upon rupture of the film, water imbibes into drained pores, compressing the gas into a smaller volume and raising its pressure. Thus, direct gas-water contact is regained and hydrate formation proceeds. This process is arrested when the hydrate film is everywhere thick enough and the gas pressure recovers to a point where the film becomes stable, causing hydrate formation to proceed in an increasingly slow rate.

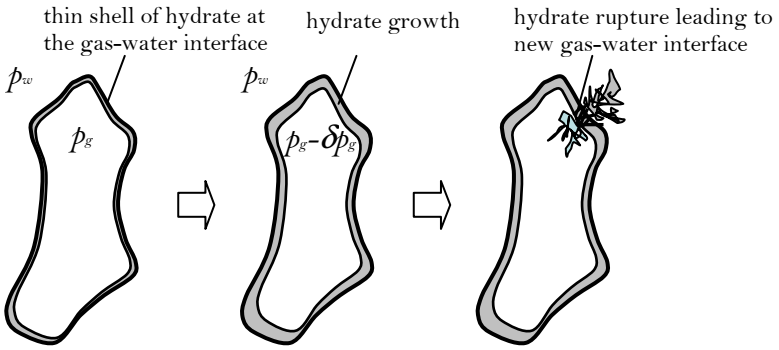

Figure 1: Hydrate precipitates as a thin layer around the gas-water interface. The volume occupied by hydrate is less than that of its stoichiometric components. Thus if the hydrate layer is rigid, the pressure inside the volume of gas will decrease, eventually leading to mechanical instability and rupture of the hydrate shell. This is a potential mechanism for enhancing the mobility of methane gas and providing additional gas-water interface area.

1. Simulations of gas invasion under hydrate-forming conditions

1.1 Gas-water interface location prior to hydrate formation

Given the different timescales associated with drainage and hydrate formation, the drainage endpoint provides the starting configuration for our simulations of hydrate growth. We find the invasion pattern using the 3-D coupled flow-mechanics model described in previous reports (e.g. Quarterly Progress Report for 1 Apr 09 – 30 Jun 09). We exclude trapping and assume that an interface, initially connected throughout the sediment, passes between all pore throats connecting drained and undrained pores. Since the capillary pressure is not sufficient to allow advancement of the interface through the narrowest part of these throats, we assume that the interface lies within the undrained side of these pore throats.

1.2 Pressure drop due to conversion of gas into hydrate

In our simulations, we increment the thickness of the hydrate film, ξ, uniformly throughout the interface. We use fixed increments $d\xi$ throughout the simulations; thus, given the increasingly slower rate of formation expected due to increasing mass-transfer limitations [Taylor *et al.*, 2007], the timesteps toward the end of the simulations are larger than those at the beginning. To compute the volume of hydrate formed at each timestep, we assume the film thickness is much smaller than its areal extent, $\xi << (A_{GWI})^{1/2}$, where A_{GWI} is the total effective film area. The incremental hydrate volume due to $d\xi$ is $dV_H = A_{GWI}\, d\xi$.

The area A_{GWI} is evaluated by summing over the areas of individual "unit" surfaces, where each surface is associated with a pore on the gas side of the meniscus, and includes two pieces: (i) a film across the pore throat (type 1), and (ii) a film coating parts of the grains that define that throat (type 2). In our 3-D model, each pore body and pore throat is defined by a tetrahedral connecting the centers of 4 grains and a triangular face made of 3 grain centers. Using analogy with hexagonal packing of spheres, the area of each surface is the sum of a film across a throat (type 1) and 3 parts of grain coating (type 2), as each type 2 part makes for 1/6 of the coating of a single spherical grain. The area of each film type is approximated by assuming that it has the shape of a hemispherical cap, making the area of each surface equal to $2\pi r_1^2 + \pi r_2^2$, where r_1 and

r_2 are the radii of the caps near a throat and coating the grains, respectively; see Figure 2. Here, $r_1 = (r_{th} + r_p)/2$, r_2 is the arithmetic average of the grain radii, r_{th} is the Haines insphere radius of the throat and r_p is the effective radius of the gas pore, evaluated by $r_p = (4/3\pi V_p)^{1/3}$ where V_p is the pore volume.

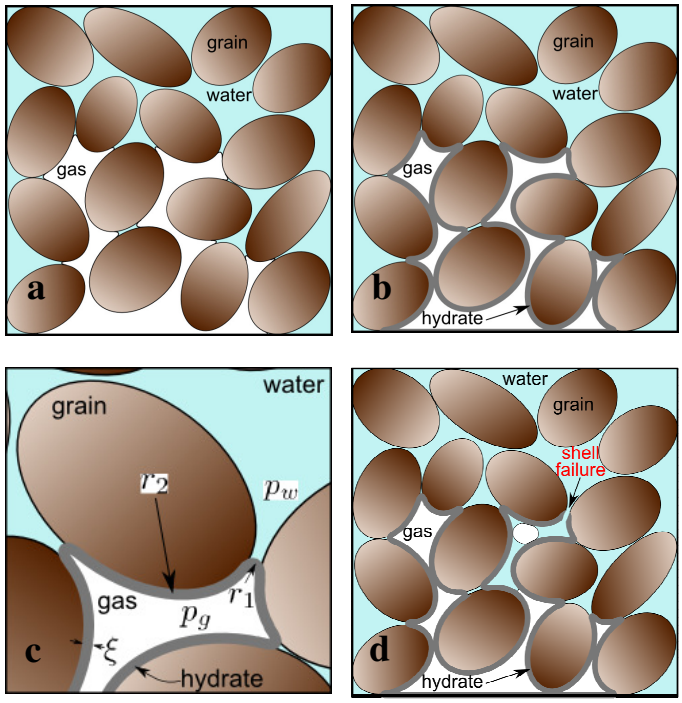

Figure 2: Schematic of hydrate growth mechanism. The starting point for the simulations is the gas-water interface location (pore occupancy at drainage endpoint) from the drainage simulations (a). A thin hydrate film grows across the interface (b). By evaluating the drop in gas pressure as it converts to hydrate, increasing the film's width, we determine the mechanical stability of the film in each pore, using linear-elastic buckling analysis (c). Upon rupture of the hydrate film, water imbibes, regaining connectivity with the gas and forming new gas-water interfaces (d). This enhances the $CH_{4(g)} \rightarrow CH_{4(aq)}$ conversion rate, which otherwise vanishes quickly due to mass-transfer limitations. Additional consequence of imbibition is trapping of gas bubbles, reducing the connectivity of the gas body.

We compute the pressure decrement due to formation using an equation of state (EOS) relating the change in gas molar content and pressure, where the number of CH_4 moles converted into hydrate at each timestep is $dn_H = \rho_H \, dV_H / M_H$. Here, ρ_H, dV_H, and M_H are the hydrate density, volume increment, and molar mass, respectively. For simplicity, we use an ideal gas EOS, $p_g V_g = n_g RT$, where p_g and V_g are the gas pressure and volume, n_g is the number of methane moles, T is the temperature, and R=8.314J/(K mol) is the gas constant. Further assumptions employed are (1) The temperature is equal to that of the sediment; (2) Isothermal conditions, neglecting the effect of latent heat; and (3) Since growth occurs into the water phase, V_g remains fixed. Under these assumptions, the pressure changes linearly with the number of moles converted to hydrate dn_g: $dp_g = dn_g RT/V_g$. Assuming complete filling of hydrate cages with methane and negligible methane dissolution in water, $dn_g = -dn_H$.

1.3 Renewal of gas-water contact by mechanical instability of the hydrate film

The mechanical stability of the films within the pore throats is evaluated using a linear buckling analysis of a spherical cap [Zoelly, 1915]. Assuming each hydrate film within a throat deforms as an isotropic, homogenous, linearly elastic body, the critical buckling pressure is $p_{cr} = [2E_H(\xi/r_1)^2]\ [3(1-\nu_H^2)]^{-1/2}$, where E_H and ν_H are Young modulus and Poisson ratio of the hydrate film. Thus, a film of curvature $1/r_1$ will fail if $p_w - p_g > p_{cr}$, where p_w is the water pressure. Assuming uniform hydrates stiffness in all pores, the film will rupture in the pore which has the smallest thickness to radius of curvature ratio, ξ/r_1. We note that imperfections such as impurities within the hydrate film can strongly reduce its strength [Ma *et al*., 2008].

1.4 Imbibition following film rupture

Once the hydrate film ruptures, the lower gas pressure allows water to imbibe into some of the drained pores. With each pore imbibed, the gas is compressed into a smaller volume thus its pressure rise. The pressure p_g is inversely proportional to the volume according to the ideal gas EOS: $p_g = p_{g,0}V_{g,0}/V_g$, where subscript *0* denotes the value prior to imbibition. We assume that the rate of water diffusing through *intact* portions of the hydrate film is negligible relative to that through the ruptured portion, and consider imbibition only at locations in which *direct* gas-water contact is regained. Considering the short timescale associated with GWI readjustments relative to that of hydrate growth, growth is not simulated during imbibition.

Since, by definition, $p_w > p_g$ at failure, the pore on the gas side of the ruptured throat is always imbibed. After that, we model pore-by-pore imbibition, computing p_g after each pore imbibed. The order in which the pores are imbibed is determined according to the equivalent pore radius (r_p) – at each step the drained pore of maximum radius among all candidates is selected. The list of imbibition candidates includes all drained pores which are in direct contact (with no intact hydrate film) with water. Assuming the water is everywhere connected, the size of the water reservoir allows us to neglect variations in water pressure.

1.5 Further hydrate growth following rupture

When imbibition is arrested, hydrate growth resumes along the freshly exposed menisci as well as along the older part of the meniscus along which hydrate rim has grown. In principle, the initial formation rate along (rate of increase in ξ) will be larger along the new menisci [Taylor *et al*., 2007]. In addition, capillary inhibition may enhance the hydrate formation rates in larger pores [Clennell *et al*., 1999]. However, our model predicts that film rupture and imbibition either occurs immediately after the film growth begins, while the film is extremely thin, or do not occur at all, allowing us to neglect the effect of the film width on the growth rate. In addition, since our numerical samples have a relatively narrow pore-size distribution, we neglect the effect of capillary inhibition, implying faster growth in larger pores [Clennell *et al*., 1999]. Therefore, we assume a uniform growth rate $d\xi$ in all pores with sufficient methane supply.

We do not simulate hydrate growth along parts of the film which are no longer in direct contact with gas – within pores that has been imbibed or previously ruptured. For the same reason, these portions are not considered as candidates for rupture. We note that, while these gas-limited pores may not play an important role in the short–term hydrate growth, they may contribute to the long-term hydrate distribution, e.g. as nucleation points for hydrate growth following gas

recharge and meniscus rearrangements. Rupture-growth-imbibition cycles are simulated until growth slows to a negligible rate due to mass transfer limitations. The mass transfer rate is considered negligible when the film thickness becomes greater than a certain threshold (here, ½ of the pore radii).

Finally, we note that for the low short-term hydrate saturations predicted by our model, the impact of latent heat and reduction in equilibrium temperature due to salt exclusion which are associated with hydrate formation, both reducing the driving force (supercooling), is negligible (less than 0.3°C). These processes are expected to significantly affect the formation rate only if the sediment *p-T* conditions are just at the thermodynamic stability limit, for instance less than 5m above the three-phase equilibrium depth for a geothermal gradient of 55°C/km.

2 Simulation results

The invasion pattern at the percolation threshold and the distribution of the hydrate throats are shown in Figure 3. These simulations were performed on two samples containing ~14,300 grains, with average grain size of 100 and 0.1μm, hereafter referred to as coarse- and find-grained. In the coarse-grained sample, the large pore sizes lead to multiple rupture-imbibition-growth cycles, increasing the number of pore throats containing a hydrate film from ~2,600 right after the drainage endpoint to ~4,100. In contrast, the hydrate film (formed in ~900 throats) in the fine-grained sample remains intact, and the gas-filled fracture is not converted into hydrate. Thus, the hydrate shell acts to preserve the gas in its own phase, and the gas body remains connected.

3 Discussion

Our model suggests that two distinct mechanisms determine the short-term methane distribution following gas invasion into marine sediment: (1) In fine-grained sediments, conversion of the gas body within gas-filled fractures diminishes quickly due to mass-transfer limitations, allowing self-preservation of the gas in its own phase; (2) In coarse-grained sediments mechanical instabilities allow renewal of direct gas-water contact and enhance mass transfer and thus hydrate formation. In addition, imbibition events which follow hydrate film rupture are expected to trap gas bubbles by snap-off, reducing gas connectivity.

The fate of the gas-filled fracture will depend on the boundary conditions indicated by the geologic settings: if gas is recharged, the well-connected (thus with high relative permeability) gas body could traverse the sediment, eventually making its way to the water column. If, on the other hand, the gas remains trapped in the fracture for longer periods with no further recharge, it will eventually convert entirely into hydrate, forming the vein-filling hydrate deposits which are frequently-encountered in fine-grained layers [Abegg *et al*., 2008; Obzhirov *et al*., 2009]. The insights gained from our grain-scale model could be used to explain the correlation between hydrate saturation and fraction of coarse-grains in the sediment [Torres *et al*., 2008].

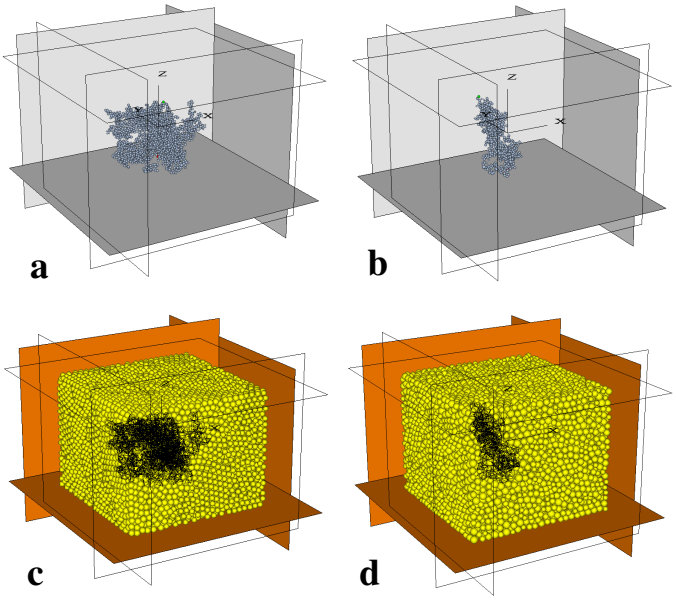

Figure 3: Results of simulations of drainage under hydrate-forming conditions in coarse- and fine-grained sediment. Top row: invasion pattern (grey spheres represent drained pores, solid grains and undrained pores not shown) at the drainage endpoint in the coarse-grained (a) and fine-grained (b) samples, with saturations of 17 and 4% and percolation pressures of 4.4KPa and 3.5MPa, respectively. Bottom row: hydrate film (black line represents a hydrate across a pore throat) formed along the gas-water interface within the coarse-grained (c) and fine-grained (d) sediment (yellow spheres represent sediment grains).

Bibliography

Abegg, F., Bohrmann, G., Freitag, J., and Kuhs, W. (2007). Fabric of gas hydrate in sediments from Hydrate Ridge—results from ODP Leg 204 samples, Geo-Mar. Lett., 27:269–277.

Clennell, M. B., Hovland, M., Booth, J. S., Henry, P., and Winters, W. J. (1999). Formation of natural gas hydrates in marine sediments: 1. Conceptual model of gas hydrate growth conditioned by host sediment properties. J. Geophys. Res., 104(B10):22985–23003.

Davies, S. R., Sloan, E. D., Sum, A. K., and Koh, C. A. (2010). In situ studies of the mass transfer mechanism across a methane hydrate film using high resolution confocal Raman spectroscopy, Journal of Physical Chemistry C, 114(2):1173-1180.

Gumerov, N. A., and G. L. Chahine (1998). Dynamics of bubbles in conditions of gas hydrate formation, 8th International Offshore and Polar Engineering Conference, Int. Soc of Offshore and Polar Eng., Montreal, Canada.

Ma, Y. Q. and Wang, C. M. and Ang, K. K. (2008). Buckling of super ellipsoidal shells under uniform pressure. Thin-Walled Structures, 46(6):584-591.

Obzhirov, A. (2009). Methane Fluxes and Gas Hydrates in the Sea Of Okhotsk. Fire in the Ice, Spring 2009, NETL.

Ribeiro, C.P. and Lage, P.L.C. (2008). Modelling of hydrate formation kinetics: state-of-the-art and future directions. Chem. Eng. Sci. 63:2007–2034.

Sloan, E. D. and Koh, C. A. *Clathrate Hydrates of Natural Gases*, 3rd Ed.; CRC Press, Taylor and Francis Group: Boca Raton FL, 2008.

Sum, A.K., Koh, C.A., and Sloan E.D. (2009). Clathrate Hydrates: From Laboratory Science to Engineering Practice. Ind. Eng. Chem. Res, 48:7457–7465.

Sun, C.Y., Chen, G.J., Ma, C.F., Huang, Q. Luo, H. and Li, Q.P. (2007). The growth kinetics of hydrate film on the surface of gas bubble suspended in water or aqueous surfactant solution. J. Crystal Growth 306:491–499.

Taylor, C.J., Miller, K.T., Koh, C.A., and Sloan, E.D. (2007). Macroscopic investigation of hydrate film growth at the hydrocarbon/water interface. Chem. Eng. Sci., 62: 6524–6533.

Torres, M.E., Wallman, K., Trehu , A.M., Bohrmann, G., Borowski, W.S., and Tomaru, H. (2004). Methane hydrate formation in turbidite sediments of northern Cascadia, IODP Expedition 311. Earth Planet. Sci. Lett., 226:225– 241.

Zoelly R. Uber ein Knickungsproblem an die Kugelschale. PhD Dissertation, TH Zurich, 1915.

National Energy Technology Laboratory

626 Cochrans Mill Road
P.O. Box 10940
Pittsburgh, PA 15236-0940

3610 Collins Ferry Road
P.O. Box 880
Morgantown, WV 26507-0880

One West Third Street, Suite 1400
Tulsa, OK 74103-3519

1450 Queen Avenue SW
Albany, OR 97321-2198

2175 University Ave. South
Suite 201
Fairbanks, AK 99709

Visit the NETL website at:
www.netl.doe.gov

Customer Service:
1-800-553-7681